nature communications

Article

https://doi.org/10.1038/s41467-025-56496-4

# Structurally convergent antibodies derived from different vaccine strategies target the influenza virus HA anchor epitope with a subset of $V_H3$ and $V_K3$ genes

Received: 5 October 2024

Accepted: 21 January 2025

Published online: 02 February 2025

Check for updates

Ting-Hui Lin[1], Chang-Chun David Lee[1], Monica L. Fernández-Quintero[1], James A. Ferguson[1], Julianna Han[1], Xueyong Zhu[1], Wenli Yu[1], Jenna J. Guthmiller[2], Florian Krammer[3,4,5,6], Patrick C. Wilson[7], Andrew B. Ward[1] ✉ & Ian A. Wilson[1] ✉

H1N1 influenza viruses are responsible for both seasonal and pandemic influenza. The continual antigenic shift and drift of these viruses highlight the urgent need for a universal influenza vaccine to elicit broadly neutralizing antibodies (bnAbs). Identification and characterization of bnAbs elicited in natural infection and immunization to influenza virus hemagglutinin (HA) can provide insights for development of a universal influenza vaccine. Here, we structurally and biophysically characterize four antibodies that bind to a conserved region on the HA membrane-proximal region known as the anchor epitope. Despite some diversity in their $V_H$ and $V_K$ genes, the antibodies interact with the HA through germline-encoded residues in HCDR2 and LCDR3. Somatic mutations on HCDR3 also contribute hydrophobic interactions with the conserved HA epitope. This convergent binding mode provides extensive neutralization breadth against H1N1 viruses and suggests possible countermeasures against H1N1 viruses.

Influenza viruses have been circulating among humans for centuries. Apart from pandemics, current seasonal influenza A viruses result in seasonal infection in over 10% of the human population and up to 650,000 deaths per year[1]. Currently, vaccines to prevent seasonal influenza virus infection must be annually updated due to antigenic drift, which enables viruses to escape from antibodies induced by previous vaccination or infection[2]. Furthermore, sporadic outbreaks of avian-origin H5N1, H7N9, and H10N8 viruses have caused serious concerns about future pandemics along with significant economic impact due to extensive infection in poultry, other birds, and mammals[3–7]. Moreover, inter-species transmission of influenza viruses from birds and mammals to humans can potentially lead to a new pandemic virus[8]. Therefore, a universal influenza vaccine capable of eliciting protective antibodies against divergent influenza viruses is an unmet need.

Hemagglutinin (HA), the major surface protein of the virus, is expressed as a homotrimer on the influenza virus and is a primary target of neutralizing antibodies. Based on antigenic diversity,

[1]Department of Integrative Structural and Computational Biology, The Scripps Research Institute, La Jolla, CA 92037, USA. [2]Department of Immunology and Microbiology, University of Colorado Anschutz Medical Campus, Aurora, CO 80045, USA. [3]Department of Medicine, Icahn School of Medicine at Mount Sinai, New York, NY 10029, USA. [4]Department of Pathology, Molecular and Cell Based Medicine, Icahn School of Medicine at Mount Sinai, New York, NY 10029, USA. [5]Center for Vaccine Research and Pandemic Preparedness (C-VARPP), Icahn School of Medicine at Mount Sinai, New York, NY, USA. [6]Ignaz Semmelweis Institute, Medical University of Vienna, Vienna, Austria. [7]Drukier Institute for Children's Health, Department of Pediatrics, Weill Cornell Medicine, New York, NY, USA. ✉e-mail: andrew@scripps.edu; wilson@scripps.edu

influenza A viruses have been classified into 18 or 19 HA subtypes (H1-H19) that can be partitioned into group 1 and group 2[9–13]. The HA is responsible for viral entry and is composed of a globular head and a stem domain[12]. The HA head domain contains the receptor binding site (RBS) that interacts – for most subtypes - with sialoside receptors on host cells and is highly diverse among subtypes; however, the stem domain is relatively conserved and houses the machinery for virus-host membrane fusion[14,15]. As a result, antibodies that bind to the head domain are usually strain-specific and highly susceptible to antigenic drift, while those that bind to the stem domain have greater cross-reactivity.

Over the past decade, influenza vaccine development has aimed to elicit broadly neutralizing antibodies (bnAbs) that can protect from different subtypes of viruses. These bnAbs can be induced by different vaccine strategies[16–20]. Beginning around 2009, several human bnAbs to influenza virus were characterized and identified[21,22]. Most of these bnAbs recognized the conserved stem domain and were able to neutralize or protect against different subtypes mainly in one of or occasionally in the two HA groups, such as the prototypic group 1 HA-specific bnAb CR6261[21], group 2-specific bnAb CR8020[23], and group 1 and 2 bnAbs CR9114 and FI6v3[24,25]. To overcome the group- and subtype-specific barrier on the stem domain, cross-reactive bnAbs to the stem domain often share similar genetic elements and critical binding motifs. The germline-encoded $V_H$1-69 bnAbs, targeting the HA stem predominantly using their heavy chain and a critical hydrophobic IF motif from HCDR2 capable of binding subtypes from group 1 and group1/group 2, respectively (e.g. CR6261 and CR9114), and are the predominant bnAbs to the HA stem isolated from multiple donors (multidonors)[21,24,26,27]. Aside from $V_H$1-69 bnAbs, germline antibodies $V_H$6-1/$D_H$3-3, $V_H$1-18/D3-9, $V_H$1-18 with a QXXV motif or $D_H$3-9 LXYFXWL in HCDR3, have exhibited molecular signatures for recognition of HAs across the two groups[28–30].

To achieve elicitation of such bnAbs through vaccination, several approaches have been pioneered, such as heterologous strain boost vaccine strategies[31–34], expansion of the breadth of antibody response by immunization with a different subtype[18], chimeric HAs (cHAs)[17,20] comprising a conserved HA stem and exotic HA heads, and headless HAs that lack the HA head and are engineered to be stable trimers[19,35].

In this work, we analyzed antibodies that were elicited with different vaccine strategies from different individuals from previous studies[36,37]. We selected four antibodies that bound to the membrane-proximal anchor region, which is lower down the stem compared to the central stem epitope[36]. Compared to multi-donor class bnAbs that use the same genetic elements for recognizing their epitopes, these antibodies have some diversity, albeit somewhat restricted, in their heavy ($V_H$3-23, $V_H$3-30, and $V_H$3-48) and light ($V_K$3-11 and $V_K$3-15) chains and with different V(D)J recombination in heavy chain complementarity-determining region 3 (HCDR3) and in light chain complementarity-determining region 3 (LCDR3). Furthermore, these antibodies have a wide spectrum of binding and neutralizing activities to the H1N1 subtype. Hence, it is important to understand how variant antibody types target key conserved epitopes in order to drive rational vaccine design. Overall, these structures provide further insight into the binding and interaction of anchor antibodies to influenza A virus HAs.

## Results

### Identification of four anchor antibodies derived from different $V_H$ germline genes

Four antibodies, 047-09_4F04, 241_2F04, 346-54, and SFV009_3G01, were elicited after vaccination either with monovalent or quadrivalent seasonal inactivated viruses (MIV, QIV) or chimeric group 1 HA (cHA) vaccines in different individuals[17,34,36–38] (Fig. 1a). To identify the epitopes and binding mode of anchor antibodies, we selected four antibodies encoded by distinct germline genes and one with the same germline as the previously published 222-1C06 anchor antibody[36] for comparison. All bind to the membrane-proximal anchor region on HA. Despite their restricted binding site, different $V_H$3 genes ($V_H$3-23, $V_H$3-30, $V_H$3-30-3, and $V_H$3-48) encode the heavy chain and are strictly paired with a restricted subset of $V_K$3 genes ($V_K$ 3-11 and $V_K$ 3-15) (Fig. 1a). These data indicate that antibodies targeting the anchor epitope are all encoded by subsets of $V_H$3 and $V_K$3 genes to date, although the $V_H$3 gene family is the largest, accounting for half of all $V_H$ genes with the greatest degree of inter-family diversity. We compared these four antibodies with antibody 222-1C06, which was isolated from a participant in a phase I clinical trial of a group 1 chimeric HA (cHA) vaccine[16,17], as its cryo-EM structure was solved at 3.4 Å in a previous study[36]. Despite some diversity in $V_H$3 and $V_K$3 gene usage, binding analysis by biolayer interferometry (BLI) of these five anchor antibodies demonstrated that they were broadly reactive to H1N1 HAs isolated from humans between 1934 and 2019, including HAs from the 2009 pandemic strain and the 2019 seasonal influenza virus vaccine strain (Fig. 1b). These anchor antibodies elicited from different vaccine strategies also exhibited neutralization in an in vitro micro-neutralization assay against these diverse H1N1 viruses (Fig. 1c). The neutralization ability varied among different H1 strains due to some minor variation in the epitope residues (Fig. 1d), especially for viruses isolated before 1977, which generally exhibited lower potency. For pre- and post-pandemic (2009) H1N1 viruses, all anchor antibodies possessed levels of neutralization (0.1-1 μg/ml) comparable to that of FI6v3 (a central stem antibody) (Fig. 1c). However, anchor antibodies rarely exhibit cross-reactive binding with other HA subtypes, except for 222-1C06, which also binds and neutralizes H2 and H5 HAs[36].

To elucidate how these antibodies bind to the anchor epitope on the HA membrane-proximal region and to analyze the precise structural features of the interactions, we determined x-ray structures of 047-09_4F04, 241_2F04, and 346-54 and a cryo-EM structure of SFV009_3G01 in complex with the H1 HA of the A/California/04/2009 (CA04) virus (Supplementary Tables 1 and 2) at resolutions ranging from 2.4 to 3.2 Å. The four antibodies bind with a highly conserved angle of approach and the mode of binding to the anchor epitope is similar to that previously described for anchor antibodies[36] (Fig. 2a).

### Structural characterization of 047-09_4F04 Fab in complex with A/California/04/09 (CA04) H1 HA

The heavy chain of the 047-09_4F04 antibody is encoded by germlines $V_H$3-48, $D_H$6-19, and $J_H$4 and paired with a light chain encoded by $V_K$3-15 and $J_K$4 (n.b. all Fab sequences are in Kabat numbering). VDJ recombination, exonuclease trimming, and 11-residue N-additions generate a HCDR3 of 15 residues (Fig. 3a, Supplementary Figs. 1 and 2). However, outside of the N-additions, the $V_H$ gene has only 7 somatic hypermutations (SHM) with ~95% residues identical to the $V_H$3-48 germline-encoded sequence (Supplementary Figs. 1 and 2). The 047-09_4F04 Fab contacts the anchor region of CA04 HA via all six CDRs, as well as LFR2 (Fig. 2b). The total buried surface (BSA) on 047-09 4F04 is 1300 Å² with 941 Å² provided from the heavy chain and 359 Å² from the light chain (Supplementary Fig. 3a). The total BSA on the HA is 1253 Å² (Fig. 2b). From the 7 SHM residues in the $V_H$ gene, five are from HCDR1 and HCDR2 (Supplementary Fig. 2a). None of the SHM residues in HCDR1 directly interact with the HA in the anchor region and only one residue (Y32) from HCDR1 interacts with the HA. However, the BSA on HCDR2 and HCDR3 is 391 Å² and 528 Å² (Supplementary Fig. 3a), which account for 42% and 56% of total BSA in the heavy chain, indicating dominance of the HCDR2 and HCDR3 interactions. Indeed, alanine scanning shows L55A in HCDR2 reduces binding to CA04 HA (Supplementary Fig. 4). SHM residue L55 contributes 160 Å² (41% of total BSA of HCDR2) and mainly contacts the lower hydrophobic pocket composed from P9 from HA1 and Y141 and I173 from HA2 (Fig. 3a). In addition, the sidechain hydroxyl group of SHM residue S56 makes hydrogen bonds with Gly10 in HA1 and E139 in HA2 and creates

https://doi.org/10.1038/s41467-025-56496-4

a

| | | Heavy chain | | | Light chain | |
|---|---|---|---|---|---|---|
| Antibody | Vaccine | $V_H$ gene | $D_H$ gene | $J_H$ gene | $V_K$ gene | $J_K$ gene |
| 047-09_4F04 | 2009 MIV | $V_H$3-48 | $D_H$6-19 | $J_H$4 | $V_K$3-15 | $J_K$4 |
| 241_2F04 | 2014 QIV | $V_H$3-23 | $D_H$5-18 | $J_H$4 | $V_K$3-15 | $J_K$5 |
| 346-54 | cHA | $V_H$3-30-3 | $D_H$3-16 | $J_H$5 | $V_K$3-11 | $J_K$4 |
| SFV009_ 3G01 | 2009 MIV | $V_H$3-30 | $D_H$3-16 | $J_H$5 | $V_K$3-11 | $J_K$5 |
| 222-1C06 | cHA | $V_H$3-48 | $D_H$3-10 | $J_H$4 | $V_K$3-15 | $J_K$4 |

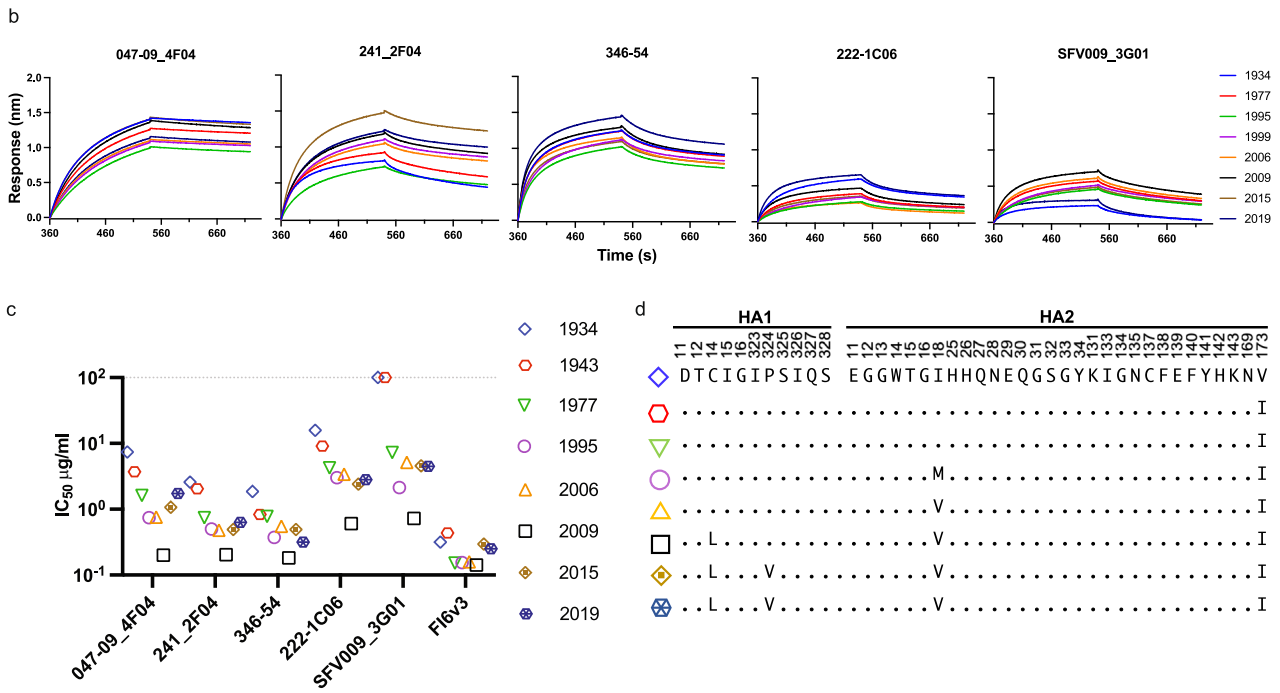


**Fig. 1 | Characterization of binding and neutralization of 047-09_4F04, 241_2F04, 346-54, SFV009_3G01 and 222-1C06 to a panel of H1N1 HA proteins and viruses spanning 90 years. a** Antibody information. V(D)J gene usage of heavy and light chains in 047-09_4F04, 241_2F04, 346-54, SFV009_3G01, and 222-1C06. 2009 MIV: monovalent 2009 pandemic H1N1 inactivated influenza vaccine; 2014 QIV: 2014-2015 quadrivalent inactivated influenza vaccine; cHA: cH8/1 and cH5/1 influenza A group 1 chimeric vaccine. **b** Binding of 047-09_4F04, 241_2F04, 346-54, SFV009_3G01, and 222-1C06 to H1N1 HAs from 1934 to 2019 using biolayer interferometry (BLI). The y-axis represents the response. **c** Neutralization using an in vitro microneutralization assay of each antibody to representative H1N1 viruses from 1934 to 2019. FI6V3, which binds the central stem of group 1 and group 2 HAs, was used as a positive control. Average $IC_{50}$ values of each antibody to H1N1 viruses were plotted as a single symbol. **d** Sequence variation in anchor epitopes among human H1N1 viruses used in binding and neutralization assays after alignment with PR8 (1934) and indicated with a letter if a residue differs from PR8 and with a dot (.) for conserved residues. Anchor epitope residues are shown for the HA1 and HA2 subunits of the HA.

a serine hydrogen bond network ($S_{52}XS_{53}XXS_{56}$) with two germline-encoded residues, S52 and S53 (Fig. 3a). When S52, S53, and S56 are substituted with alanine, the binding affinity was drastically reduced (Supplementary Fig. 4), indicating a role for these serine residues in binding of 047-09_4F04 Fab to HA. In HCDR3, four residues from the $D_H$6-19 germline ($G_{99}YSS_{100b}$) along with two residues ($F_{100c}F_{100d}$) that are junction-encoded (57% of total BSA of HCDR3) target the upper pocket of the anchor epitope and make hydrophobic interactions and sidechain hydrogen bonds with I326 and I329 from HA1 and E11, W14, H25, Y34, and N135 from HA2 (Fig. 3a and Supplementary Fig. 8d). Structural analysis reveals that the germline-encoded Y100 directly inserts into a gap between the cleavage loop at the C-terminus of HA1 and the fusion peptide of HA2 and hydrogen bonds with E11, which stabilizes the HCDR3 conformation and allows F100c to insert into the upper hydrophobic pocket (Fig. 3a). The structural data are consistent with the alanine scanning results showing that binding is dramatically reduced when Tyr100 is replaced with Ala (Supplementary Fig. 4).

The light chain of 047-09 4F04 antibody is encoded by $V_K$3-15 and $J_K$4, with 98.6% identity to germline and only three SHMs (Fig. 4a and Supplementary Figs. 1 and 5a). The BSA on LCDR3 is 222 Å², which accounts for 59% of the total BSA in the light chain (Supplementary Fig. 3a). Y92, the only SHM in LCDR3, hydrogen bonds with G16 in the fusion peptide (Fig. 4b). In addition, most of the residues involved in the interaction between light chain CDR loops and HA are germline-encoded (Supplementary Fig. 5a). This observation further highlights the importance of germline-encoded residues in the light chain for binding to HA.

## Structural characterization of 241_2F04 Fab in complex with A/California/04/09 (CA04) H1 HA

Antibody 241_2F04 was isolated from an individual vaccinated with the 2014 quadrivalent seasonal inactivated vaccine (Fig. 1a). The heavy chain of 241_2F04 is encoded by germline $V_H$3-23, $D_H$5-18, and $J_H$4 and paired with a light chain encoded by $V_K$3-15 and $J_K$5 (Fig. 1a). The identity of the $V_H$ gene to the inferred germline gene is 96%, with 8 SHM residues (Supplementary Figs. 1 and 2). Among the 15 residues in HCDR3, two appear to be from SHM, and 9 from N-additions (Fig. 3b). 241_2F04 interacts with anchor region of CA04 HA via HCDR2 and HCDR3 from the heavy chain and LCDR1 and LCDR3 from the light chain (Fig. 2b, Supplementary Figs. 2b and 5a). The total BSA on 241_2F04 is 946 Å², with 756 Å² from the heavy chain and 190 Å² from the light chain (Supplementary Fig. 3b). The total BSA on HA is 920 Å²,

https://doi.org/10.1038/s41467-025-56496-4

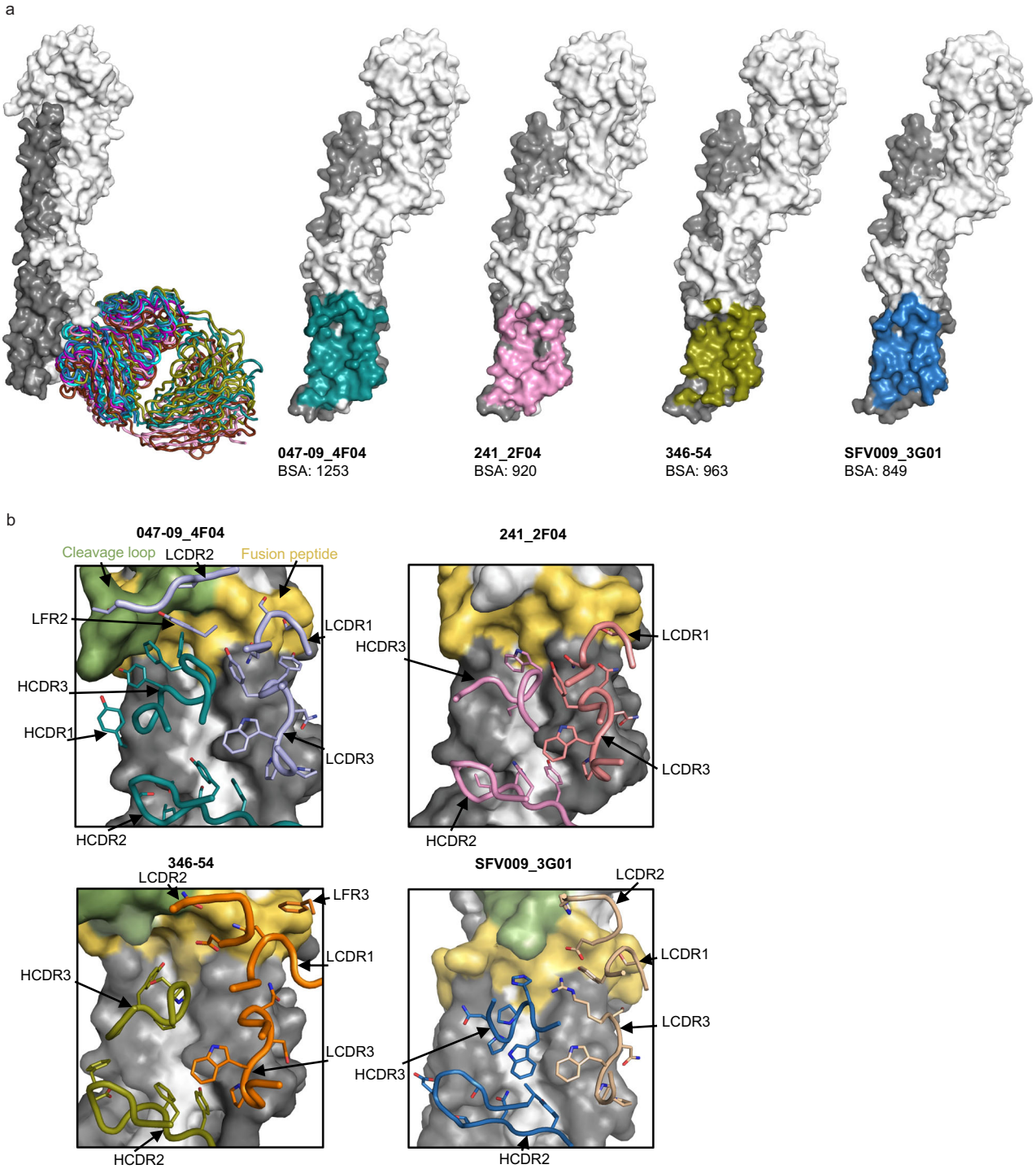


**Fig. 2 | The anchor epitope on H1N1 HA.** An HA protomer is shown as a molecular surface with white for HA1 and gray for HA2 and antibody Fabs in different colors. **a** Alignment of 047-09_4F04, 241-2F04, 346-54, SFV009_3G01, 222-1C06, FISW84, and 204-1B06 HA-Fab complexes illustrating the conserved mode of binding to the anchor epitope at the base of the HA. Epitopes of 047-09_4F04, 241_2F04, 346-54, and SFV009_3G01 are shown in different colors. The Buried Surface Area (BSA) in Å² on the HAs by the antibodies are presented below each structure. **b** Structural characterization of each Fab in complex with A/California/04/2009 (CA04) HA. The Fab is represented by the interacting complementarity-determining regions (CDRs) and framework region (FR) in tubes with stick sidechains from heavy and light chains. The interacting CDRs and FR from the heavy and light chain are shown in teal and lavender for 40709_4F04, pink and salmon for 241-2F04, deep olive and orange for 346-54, and sky blue and wheat for SFV009_3G01. CDR loops and FR involved in HA contacts are labeled.

which is smaller than 047-09_4F04 (Fig. 2a). Thus, the binding of 241_2F04 to HA is again dominated by the heavy chain. Moreover, HCDR2 contributes slightly more BSA than HCDR3 (Supplementary Fig. 3b). Residues from the $V_H$3-23 germline also form a serine hydrogen bond network ($S_{52}XS_{53}XXS_{56}$), similar to 047-09 _4F04 where S56 in HCDR2 arises from the germline gene. SHM residue I55 contributes 156 Å² BSA (38% of total BSA of HCDR2) and interacts with the lower hydrophobic pocket (Supplementary Figs. 3b and 8d). The contribution of BSA and interaction to HA from I55 in 241 2F04 is nearly the same as L55 in 047-09 4F04, which is also somatically mutated from the inferred germline gene and the binding substantially diminished when substituted with alanine (Supplementary Fig. 4). In HCDR3, the

https://doi.org/10.1038/s41467-025-56496-4

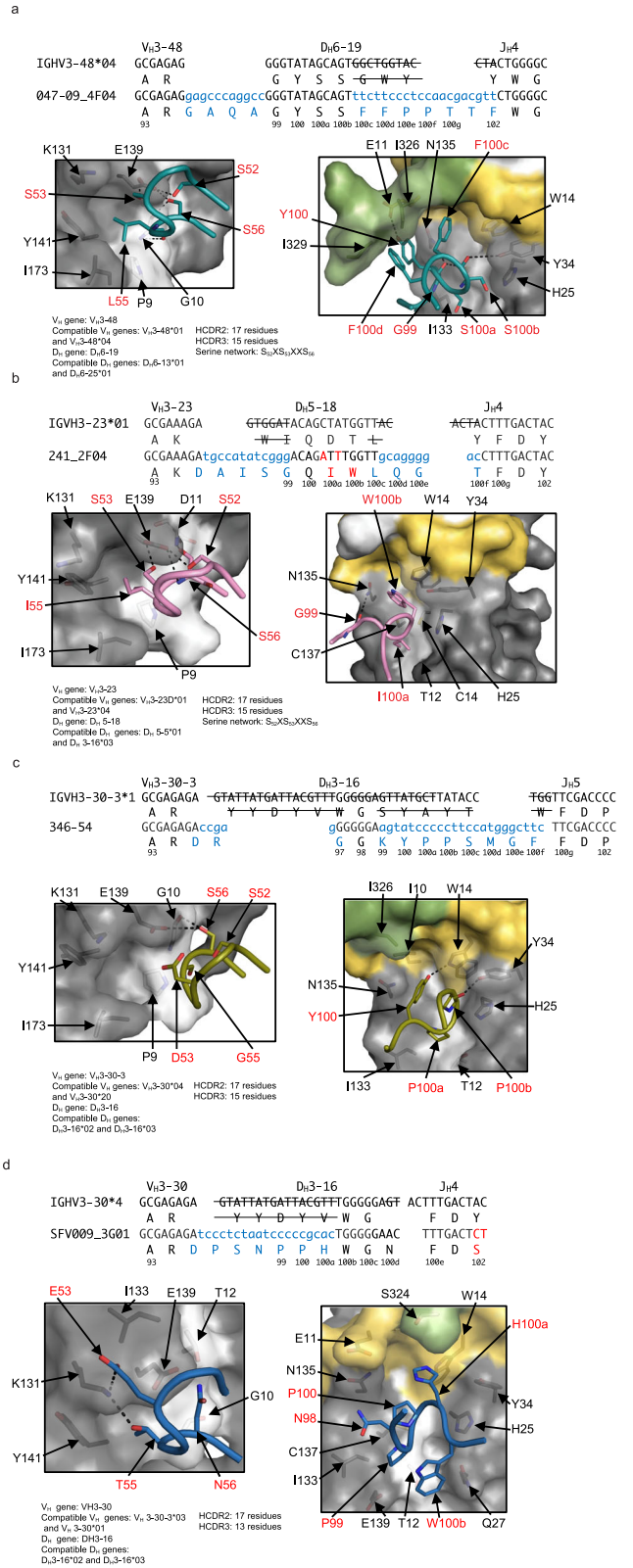


**Fig. 3 | Germline gene usage in the heavy chain and structural characterization of anchor antibodies in complex with CA04 HA.** Germline gene-encoded nucleotides and amino acids are shown in black, and N-additions in junction-encoded residues are in blue. Nucleotides removed by exonuclease are indicated with a line across the letter. Kabat numbering is used for Fabs throughout this paper. For clarity, HA and Fab residues are colored with black and red numbers, respectively. Gene compatibility for heavy and light chain were analyzed by their nucleotide sequences in IgBlast. The CA04 HA is shown as a molecular surface with white for HA1 and gray for HA2. The fusion peptide at the N-term of HA2 and the cleavage peptide at the C-term of HA1 are depicted in yellow and green, respectively. Residues involved in side-chain and backbone interactions between HA and Fab CDRs and FR are shown as sticks and labeled. Hydrogen bonds and salt bridges are indicated with black dashes. Germline gene utilization and lengths of HCDR2 and HCDR3 loops are depicted for each Fab. **a** Germline genes $V_H$3-48, $D_H$6-19, and $J_H$4 are used in HCDR3 in 047-09_4F04. Residues involved in the interaction between heavy chain and HA in 047-09_4F04-HA complex are shown. The compatible alleles for $V_H$3-48*04 and $D_H$6-19 are presented. **b** Germline genes $V_H$3-23, $D_H$5-18, and $J_H$4 are used in HCDR3 in 241_2F04. Residues involved in the interaction between heavy chain and HA in 241_2F04-HA complex are shown. The compatible alleles for $V_H$3-23*01 and $D_H$5-18 are shown. **c** Germline $V_H$3-30-3, $D_H$3-16, and $J_H$5 gene-encoded nucleotides and N-additions for HCDR3. Residues involved in the interaction between heavy chain and HA in 346-54-HA complex are indicated. The compatible alleles for $V_H$3-30-3*01 and $D_H$3-16 are presented. **d** Germline $V_H$3-30, $D_H$3-16, and $J_H$4 gene-encoded nucleotides for HCDR3. Residues involved in the interaction between heavy chain and HA in SFV009_3G01-HA complex are presented. The compatible gene alleles for $V_H$3-30 and $D_H$3-16 are shown.

somatically mutated I100a and W100b (132 Å² and 180 Å² BSA, 90% of total BSA of HCDR3) target the upper and middle hydrophobic pockets, which are comprised of T12 and C16 from HA1 and W14, H25, Y34, and C137 from HA2 (Fig. 3b, Supplementary Fig. 3b and 8d). Alanine scanning also demonstrates that hydrophobic residues, I100a and W100b, are important for the interaction with CA04 HA (Supplementary Fig. 4).

The light chain of 241_2F04 antibody is from $V_K$3-15 and $J_K$5, with 98% identity to germline and only two SHMs (Fig. 4a and Supplementary Figs. 1 and 5a). The light chain interacts with the HA anchor region through LCDR1 and LCDR3. The BSA on LCDR3 is 176 Å² (Supplementary Fig. 3b), which accounts for 92% of total light-chain BSA, indicating most interactions between the light chain and HA are from LCDR3. Compared to Y92 from SHM in 047-09 4F04, the germline-encoded N92 in 241_2F04 makes a backbone hydrogen bond with S32 from HA2 (Fig. 4b). Of note, all light chain contact residues are encoded by the $V_K$3-15 germline (Supplementary Fig. 5a).

## Structural characterization of 346-54 Fab in complex with A/California/04/09 (CA04) H1 HA

Apart from the anchor antibodies that were elicited by seasonal influenza vaccination, 346-54 was isolated from the influenza A group 1 cHA vaccine clinical trial (Fig. 1a), where the chimeric HA consists of head domains from H5, and H8 atop a constant stem domain from H1. The heavy chain is putatively derived from the recombination of $V_H$3-30-3, $D_H$3-16, and $J_H$5 germline genes to generate a 15-residue HCDR3 and paired with a light chain derived from $V_K$3-11 (Fig. 3c, Supplementary Figs. 2 and 5b). Among the four anchor antibodies, 346-54 contains the most SHM residues (11 residues in $V_H$), with 93% identity to $V_H$3-30-3 germline sequence (Supplementary Figs. 1 and 2). The 346-54 antibody contacts the anchor region of CA04 HA via HCDR2 and HCDR3 from the heavy chain and LCDR1, LCDR3, and LFR3 from the light chain (Fig. 3c, Supplementary Figs. 2 and 5b). The total BSA on 346-54 and HA are 968 Å² and 963 Å² (Fig. 2a and Supplementary Fig. 3c). The germline-encoded D53 in HCDR2, unlike the S53 in the serine hydrogen bond networks in 047-09 4F04 and 241 2F04, does not make a direct hydrogen bond with HA (Fig. 3c); thus, the serine hydrogen bond network is decreased with only S56 making hydrogen bonds in HCDR2. Instead of hydrophobic residues L55 and I55 in 0647-09 4F04 and 241 2F04 (41% and 38% Å² of total BSA of HCDR2), G55 contributes only 53 Å² BSA (19% of total BSA of HCDR2) and does not make hydrophobic interactions with the lower hydrophobic pocket (Fig. 3c). These findings are consistent with alanine scanning (Supplementary Fig. 4) and provide insights into the importance of different SHM residues in HCDR2 that show some variation in anchor epitope recognition. HCDR3, like 241_2F04, binds to the upper and

https://doi.org/10.1038/s41467-025-56496-4

a

```
                        VK3-15                    JK4
IGKV3-15*01 CAGCAGTATAATAACTGGCCTCC -GCTCACT
            Q  Q  Y  N  N  W  P       L  T
047-09_4F04 CAGCAGTATTATAACTGGCCTCCc CTCACT
            Q  Q  Y  Y  N  W  P  P    L  T
            89          93 94 95 95a      97

                        VK3-15                    JK5
IGKV3-15*01 CAGCAGTATAATAACTGGCCTCC GATCACC
            Q  Q  Y  N  N  W  P  P    I  T
241_2F04    CAACAGTATAATAACTGGCCTCCG ATCACC
            Q  Q  Y  N  N  W  P  P    I  T
            89          93 94 95 95a      97

                        VK3-11                    JK4
IGKV3-11*01 CAGCAGCGTAGCAACTGGCCTCC GCTCACT
            Q  Q  R  S  N  W  P  P    L  T
346-54      CAACAGCGGAACAACTGGCCTCCG CTCACT
            Q  Q  R  N  N  W  P  P    L  T
            89          93 94 95 95a      97

                        VK3-11                    JK5
IGKV3-11*01 CAGCAGCGTAGCAACTGGCCTCC GATCACC
            Q  Q  R  S  N  W  P  P    I  T
SFV009_3G01 CAGCAGCGTAGCAACTGGCCTCCG ATCACC
            Q  Q  R  S  N  W  P  P    I  T
            89          93 94 95 95a      97
```

b

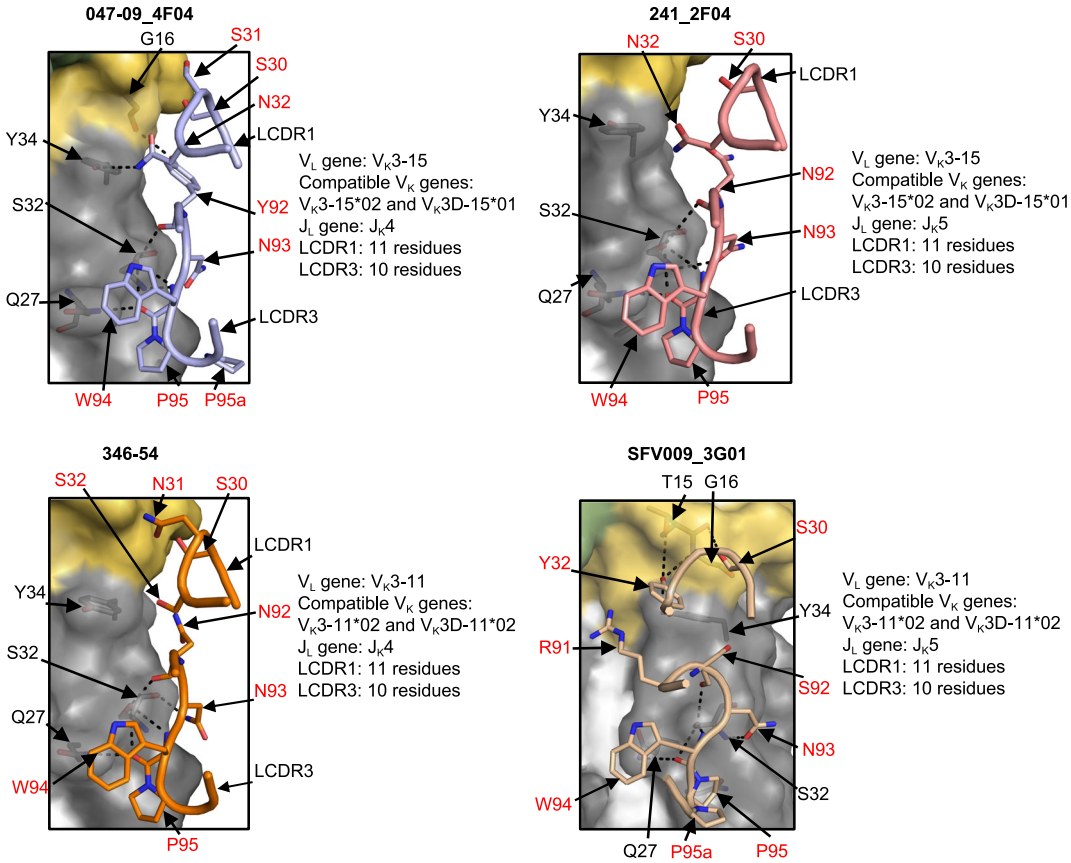


**Fig. 4 | Germline gene usage in the light chain and structural characterization of anchor antibodies in complex with CA04 HA.** The annotation for the HA and CDR sequences follows Fig. 3. Germline gene utilization and lengths of the LCDR1 and LCDR3 loop are depicted for each Fab. **a** Germline gene VK3-15 contributes to LCDR3 in 047-09_4F04 and 241_2F04, while VK3-11 encodes LCDR3 in 346-54 and SFV009_3G01. $J_K4$ gene-encoded nucleotides are used for 047-09_4F04 and 346-54, whereas $J_K5$ gene-encoded nucleotides are used for 241_2F04 and SFV009_3G01. **b** Structural characterization of Fab-HA complexes. Binding interactions to HA through LCDR1 and LCDR3 residues from the light chain are shown.

middle pockets mainly via hydrophobic interactions from hydrophobic residues, Y100, P100a, and P100b (82% of total BSA of HCDR3) from N-addition junction-encoded residues (Fig. 3c).

The light chain of the 346-54 antibody is encoded by $V_K$3-11 and $J_K$4, with 94% identity to germline and 7 SHM residues (Fig. 4a and Supplementary Fig. 1), four of which are in LCDR loops (Supplementary Fig. 5b). The light chain interaction involves LCDR1, LCDR2, LFR3, and LCDR3 (Fig. 2b). LCDR3 contributes 222 Å$^2$ (67% of total BSA in the light chain), with a similar binding mode to 047-09 4F04 and 241_2F04 (Supplementary Fig. 3c and Fig. 3).

### Structural characterization of SFV009_3G01 Fab in complex with A/California/04/09 (CA04) H1 HA

The fourth antibody, SFV009_3G01, encoded by $V_H$3-30 and $V_K$3-11, was isolated from a subject vaccinated with the 2009 monovalent seasonal influenza vaccine (Figs. 1a and 3d). Germline genes $V_H$3-30, $D_H$3-16, and $J_H$4 were used to generate HCDR3. In the cryo-EM structure, the antibody interacts with CA04 H1 HA via HCDR2, HCDR3, LCDR1, LCDR2, and LCDR3 (Fig. 2b). The total BSA on SFV009_3G01 (905 Å$^2$) is comparable to 346-54 (938 Å$^2$), with 587 and 318 Å$^2$ contributed from the heavy chain and light chain, respectively (Supplementary Fig. 3 d). The total BSA on HA is 849 Å$^2$ (Fig. 2a). Compared to 346-54 with SHM residue G55, T55 in HCDR2 like L/I55 in 047-09_4F04, 222-1C06, and 241_2F04 makes hydrophobic interactions with residues in the lower pocket (Fig. 3d and Supplementary Fig. 8d). This finding further demonstrates the preference for hydrophobic residues at residue 55. Furthermore, N-addition residues P99 and P100 along with D-gene-encoded W100b, which contribute 199 Å$^2$ BSA in HCDR3 (~73% BSA in HCDR3) (Supplementary Fig. 3d), mainly contact hydrophobic residues in the upper and middle hydrophobic pockets in the anchor epitope (Fig. 3d and Supplementary Fig. 8d).

SFV009_3G01 is encoded by $V_K$3-11 and $J_K$5 generates LCDR3 (Supplementary Figs. 1 and 5b). Like the other antibodies, LCDR3 in SFV009_3G01 accounts for the majority of the light-chain binding with a similar binding mode to the HA as the other antibodies (Supplementary Fig. 3d). Although the $V_K$ gene usage is the same as 346-54, the germline-encoded Y32 in LCDR1, instead of S32 in 346-54, makes a sidechain hydrogen bond with T15 and hydrophobic interaction with Y34 in HA2 (Fig. 3d). Overall, the sequence in the light chain in SFV009_3G01 is akin to 346-54 but the binding involves more hydrophobic interactions.

### Critical NWPP motif in LCDR3

These antibodies all bind to the anchor region via a similar restricted mode that seems to be primarily dictated by LCDR3. This finding suggests that only a few germline $V_K$ and $J_K$ genes can be engaged for anchor antibodies. The similarity of LCDR3 in each anchor antibody to its germline gene ranges from 93 to 99% (Supplementary Fig. 1). Despite some variation in V gene usage, all anchor antibodies discovered in a previous study[36,39,40] have a consistent 10-residue LCDR3 and contain an $N_{93}WPP_{95a}$ motif, suggesting their importance (Supplementary Figs. 1 and 5). Analysis of germline gene usage in LCDR3 among these five antibodies with crystal or cryo-EM structures and available DNA sequences, the NWP are germline-encoded and P95a in 047-09_4F04 and 222-1C06 appears to arise from direct joining of $V_K$3-11 or $V_K$3-15 with $J_K$4 or $J_K$5 (Fig. 4 and Supplementary Fig. 5a, b). Furthermore, this motif binds to the same position on HA via a W-shape conformation in all anchor antibodies, including FISW84 and 204-1B06 (Fig. 5a). P95a has little or no BSA on the HA, but P95 and P95a adopt cis peptide conformations and stabilize the particular conformation of LCDR3 in the NWPP region (Fig. 5a). This NWP motif with germline-encoded Y98 from HCDR2 in 222-1C06 that mediates the binding to conserved β-strands in HA was also demonstrated previously[36]. When we substituted residues in NWPP with alanine, the binding affinity was either dramatically reduced or abolished (Fig. 5f).

To decipher why A95a could cause such a dramatic effect on binding to HA, we determined an apo crystal structure with A95a in 241_2F04 (241_2F04-A95a). After superimposition of 241_2F04-A95a onto 241_2F04-HA complex, we observed a substantial movement in the NWPP region, with W94 flipping ~ 90° as the cis conformation at A95a was now abolished (Fig. 5b). The flipped W94 would then be close to HCDR3 likely perturbing the conformation of HCDR3, which resulted in a slight reduction in protein stability in a thermal shift assay (Fig. 5b and e). In addition, we found when we modeled this movement with the HA that it would cause a molecular clash between W94 of 241_2F04-A95a and Q27 of HA (Fig. 5c). When we also compared the structure of the 241_2F04-HA complex with that of 241_2F04-Apo (unliganded Fab), we found that the conformation of NWPP motif is nearly identical and HCDR3 is similar (Fig. 5d). These observations further emphasize the importance of the conformation and residues in the NWPP motif in antibody binding to the HA anchor region.

### Role of hydrophobic residues in anchor antibody CDR loops

The light chain CDR3 seems to be a dominant factor in determining the binding mode of anchor antibodies due to the conserved NWPP motif in the 10-residue LCDR3. However, the heavy chain CDR3 dominates in terms of BSA (270-528 Å$^2$ for HCDR3 vs 171-222 Å$^2$ for LCDR3, Supplementary Fig. 3). The HCDR3 sequence in these anchor antibodies is quite diverse and ranges in length from 13–15 residues (Fig. 3) The diversity of D-gene usage and VDJ recombination in HCDR3 therefore results in different residues being involved in the interaction with the upper and middle anchor region (Fig. 3 and Supplementary Fig. 8). In a previous study, two D gene-encoded motifs translated from different open reading frames of $D_H$3-9 in S9-3-37 (LGYFDWL motif) and 31.b.09 (ILTG motif) antibodies still recognized the same central stem pocket on HA stem[30]. Here, our structures reveal that different and similar $D_H$ genes can be used in these antibodies. Although 241_2F04 and 346-54 have different HCDR3 sequences (Supplementary Fig. 2), the binding of HCDR3 to HA is primarily through hydrophobic interactions from different SHMs or N-addition junction-encoded residues, resulting in similar binding modes (Fig. 6a, b). I100a and W100b in 241_2F04 and Y100, P100a, and P100b in 346-54 occupy similar upper and middle hydrophobic pockets in the anchor epitope (Fig. 6b). Notably, HCDR3 of 222-1C06, utilizing the $D_H$3-10 gene, contacts HA with the same HCDR3 region via W99 and P100 and shares a similar binding conformation as 241_2F04 and 346-54 (Supplementary Fig. 6a, c). When binding to HA, however, HCDR3 of 047-07_4F04 adopts a similar overall HCDR3 conformation around positions 100a and 100b as 241_2F04 and 346-54, but these residues are now S100a and S100b (Fig. 6b). However, the two N-addition junction-encoded residues, F100c and F100d (see also Fig. 3a), make hydrophobic interactions with I325 and I326 from the C-term cleavage loop of HA1 and W14 from the fusion peptide in HA2 (Fig. 3a, b). In SFV009_3G01, P99, P100, and W100b adopt a different conformation in CDR3 but also access the upper and middle pockets.

Moreover, we further analyzed other anchor antibodies, FISW84, published in 2018, and 204-1B06, published more recently[39,40]. Both antibodies bind to the upper or middle pockets via a single hydrophobic residue (Supplementary Fig. 6c). To evaluate the importance of these hydrophobic residues for HCDR3 binding to these pockets, we performed the alanine scanning on these residues. The binding affinity was reduced when hydrophobic residues in CDR H3 were substituted with the smaller aliphatic alanine in 047-09_4F04 and 241_2F04 (Fig. 6c). Moreover, alanine substitutions in HCDR3 more dramatically affected the binding to HA in 346-54 and eliminate binding in SFV009_3G01 and 222-1C06 (Fig. 6c, Supplementary Figs. 4 and 6). These observations show that the upper and middle pockets are the main targets for HCDR3 in anchor antibodies and that hydrophobic residues are important for engaging those pockets.

https://doi.org/10.1038/s41467-025-56496-4

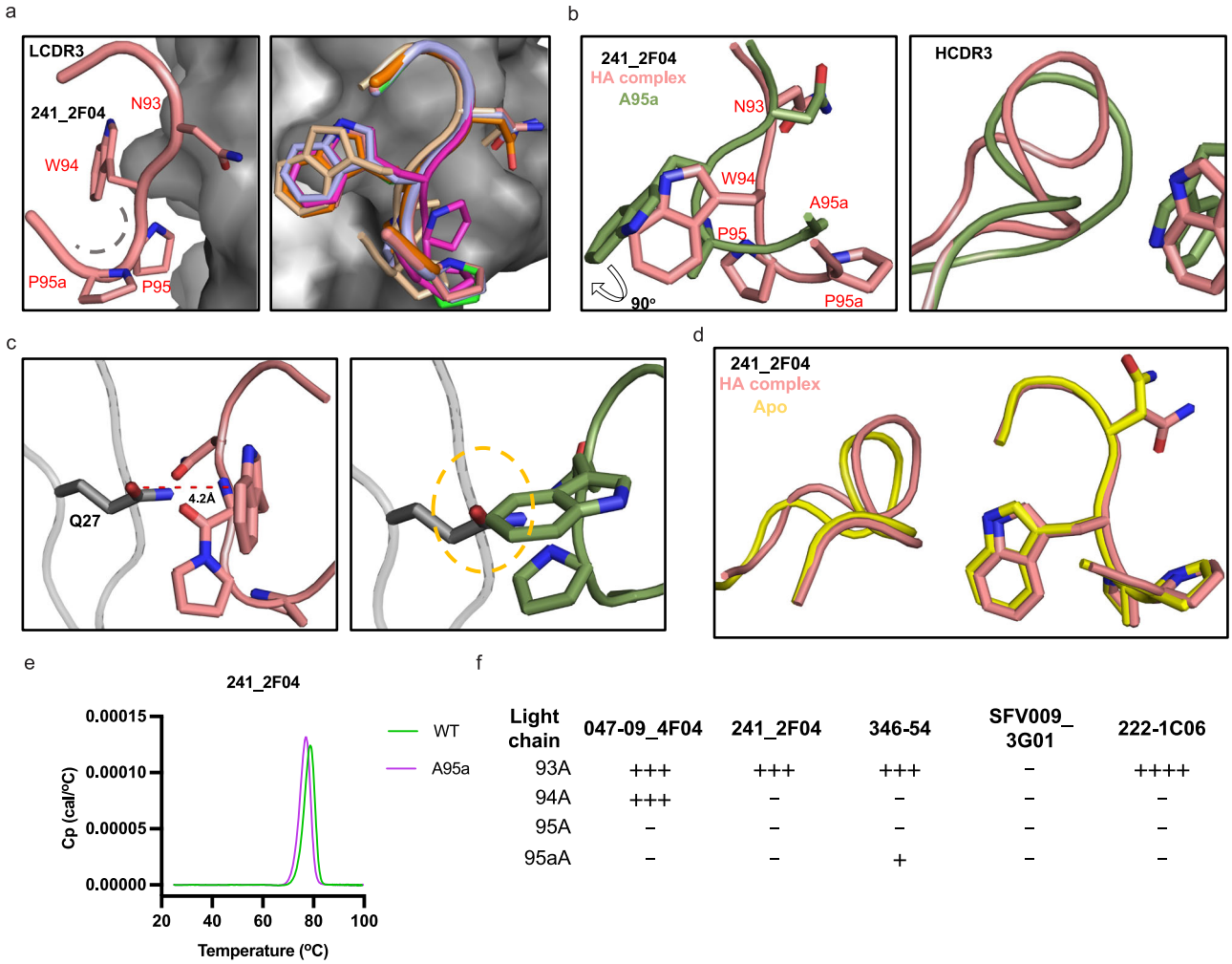


**Fig. 5 | Critical NWPP recognition motif in LCDR3 in anchor antibodies. a** Left. LCDR3 from 241_2F04 is used as an example. The rigid conformation of the proline-proline cis conformation is indicated as gray dashes. Right. Superimposition of LCDR3 from each anchor antibody. LCDR3 is depicted as a backbone cartoon with sidechains as sticks with light blue for 047-09_4F04, pink for 241_2F04, orange for 346-54, wheat for SFV009_3G01, purple for 222-1C06 (PDB: 7T3D), green for FISW84 (PDB: 6HJP), and cyan for 1B06 (PDB: 8D21). **b** Structural effect of alanine substitution of P95a in LCDR3. 241_2F04-A95a is shown as dark green and WT as pink. The overall conformation of LCDR3 in 241_2F04-A95a was superimposed onto the 241_2F04-CA04 complex. The curved arrow indicates the change in the backbone conformation that affects the conformation of W94. **c** Comparison of the distance between W94 in 241_2F04-HA and Q27 in HA2. The distance was measured by PyMol. The 241_2F04-A95a Fab structure (green) was superimposed onto 241_2F04-HA complex (pink) to determine distances. The yellow dashed circle represents as potential clash. **d** Superimposition of 241_2F04-HA with 241-Apo. The 241-Apo Fab is shown in yellow. **e** Thermal stability assay of 241_2F04-WT and 241_2F04-A95a Fabs by differential scanning calorimetry (DSC). **f** Alanine scanning of critical residues in LCDR3. The binding affinity of each mutant to CA04 HA was measured by BLI. +++++, $K_D$ < 1 nM; ++++, $K_D$ = 1-10 nM; +++ $K_D$ = 10-100 nM; ++, $K_D$ = 100-1000 nM; +, $K_D$ = > 1000 nM; -, No binding. These data are related to Supplementary Fig. 4. Sensorgrams for binding are shown in Supplementary Figs. 11–14.

Aside from these hydrophobic residues in HCDR3, hydrophobic residues in the light chain are also important for binding. As discussed in the previous section, residues in the NWPP motif in HCDR3 are critical for binding. However, the hydrophobic interactions extend from LCDR3 W94, P95, P95a, and L/I 96 to HCDR2 conserved residue Y58 along with Y50 from 047-09_4F04, H50 from 241_2F04, F50 from 346-54, and V50 from SFV009_3G01. Inter- and intra-CDR hydrophobic and aromatic interactions, including pi-pi interactions between Y/H/F50 and W94, seem to stabilize the CDRs and define the mode of recognition to HA (Fig. 6a). In addition, HCDR2 Y58 and LCDR3 W94 form an aromatic pocket with W100b from HCDR3 in 3G01, further rigidifying the conformation among HCDR2, HCDR3, and LCDR3. These interactions also include P100e and P100f from HCDR3 and Y91 from LCDR3 in 047-09_4F04, creating further inter-CDR interactions (Fig. 6a). Furthermore, 222-1C06, FISW84, and 204-1B06 also have equivalent interactions with aromatic residues at HCDR2 residues 50 and 58 for 222-1C06, FISW84 and residues 47 and 58 for 204-1B06 that make hydrophobic and aromatic interactions with LCDR3 (Supplementary Fig. 6b).

## Functional complementation of $V_K$3-11 and $V_K$3-15 with a subset of $V_H$3 heavy chains

The crystal structures of anchor Fab-HA complexes in our study reveal a similar binding mode of the light chain among all antibodies. The constrained binding mode in the light chain appears to limit the heavy chain to $V_H$3-23, $V_H$3-30, and $V_H$3-48 germline-encoded heavy chains. The similarity of the gene sequence between $V_K$3-11 and $V_K$3-15 is very high, with only five residues that differ within their CDR loops and nine total (Supplementary Fig. 5c). We therefore further tested for functional complementation by exchanging the light chain amongst these antibodies resulting in five different pairings (346-54$V_H$ with 047-09_4F0$V_K$, 047-07_4F04$V_H$ with 346-54$V_K$, 241_2F04$V_H$ with 346-54$V_K$, SFV009_3G01$V_H$ with 047-09_4F04$V_K$, and 222-1C06$V_H$ with 346-54$V_K$). All pairings were successfully expressed and retained binding to CA04

https://doi.org/10.1038/s41467-025-56496-4

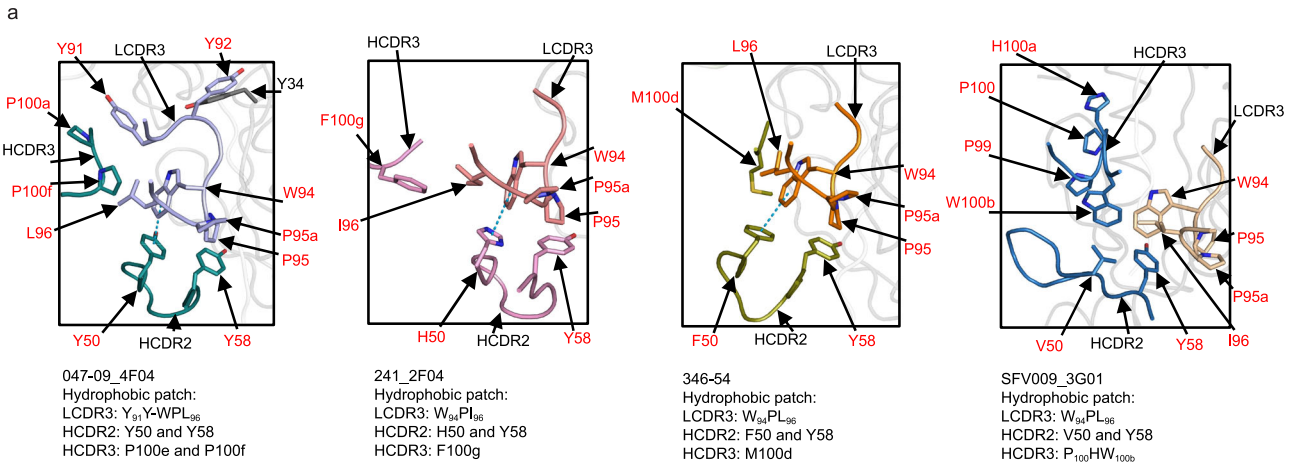


c

| Heavy chain | 047-09_4F04 | 241_2F04 | 346-54 | SFV009_3G01 | 222-1C06 |
|---|---|---|---|---|---|
| WT | ++++ | ++++ | ++++ | +++ | +++ |
| 99A | | | | - | - |
| 100A | | | - | - | - |
| 100aA | ++++ | +++ | + | | |
| 100bA | +++++ | +++ | +++ | - | |
| 100cA | ++++ | | | | |

**Fig. 6 | Comparison of hydrophobic interaction in HCDR2, HCDR3, and LCDR3 among 047-09_4F04, 241_2F04, 346-54, and SFV009_3G01 in complex with CA04 H1 HA.** CA04 HA is shown with white for HA1 and gray for HA2. **a** Residues involved in hydrophobic interactions from the CDR loops are represented in sticks and labeled. A pi-pi interaction is shown as blue dashes. **b** Key residues involved in the interaction between HCDR3 and upper and middle hydrophobic pockets in HA are indicated as sticks on CDR backbone tubes. **c** Binding affinity of each Fab with alanine substitutions for residues interacting with upper hydrophobic pocket in HA. +++++, $K_D$ < 1 nM; ++++, $K_D$ = 1-10 nM; +++ $K_D$ = 10-100 nM; ++, $K_D$ = 100-1000 nM; +, $K_D$ = > 1000 nM; -, No binding; gray background, residues not involved in HA interaction. These data are related to Supplementary Fig. 4. Sensorgrams for binding are shown in Supplementary Figs. 11–14.

H1 HA, albeit with different binding kinetics, except for 222-1C06$V_H$ with 346-54$V_K$ with no binding (Supplementary Fig. 7). However, 222-1C06$V_H$ with 346-54$V_K$ showed weak binding to A/Michigan/45/2015 H1 HA (Supplementary Fig. 7). Overall, these results indicate that anchor antibodies with $V_H$3-23, $V_H$3-30, $V_H$3-30-3, and $V_H$3-48 heavy chains seem to be compatible with $V_K$3-11 or $V_K$3-15 light chains.

## Epitope analysis of anchor antibodies

The central stem epitope, mainly comprised of residues 36-43 and 316-320 in HA1 and helix A in HA2, is the major target for the most bnAbs, such as CR9114, to the HA stem (Supplementary Fig. 8a). The anchor epitope is lower down the HA stem closer to the membrane and only one residue overlaps between the CR9114 and 047-09_4F04 epitopes: fusion peptide residue V18 in HA2. However, the epitope of group 2 specific antibody, CR8020, which recognizes the lower stem and one side of the central stem, has several residues that overlap with the anchor epitope including residues 25-36 in the B-strand in HA2 and two residues at C-terminal helix in HA1 (Supplementary Fig. 8b, c). Epitope alignment from each anchor antibody reveals that these antibodies bind to a similar region (Fig. 2a). Despite some overlap, most of the epitope is unique to anchor antibodies (Fig. 2a and Supplementary Fig. 8c). To evaluate the functional consequences of mutation of critical binding residues in HA2 for anchor antibodies, we performed alanine scanning for corresponding residues within HCDR2, HCDR3, and LCDR3 contacts (Fig. 7a). We selected W14, H25, and I133, which provide most of the hydrophobic interactions with HCDR3 in the upper and middle hydrophobic pockets, and Y141, which makes a major hydrophobic contact with L/I55 in HCDR2 in 047-07_4F04 and 241_2F04 in the lower hydrophobic pocket (Fig. 3a and b). Alanine substitutions were also made at Q27, S32, and Y34, which contribute to several backbones and side-chain hydrogen bonds with LCDR3. The anchor antibodies lost major contact with the HA when W14 and Y34 were substituted with alanine (14A, 34A) (Fig. 7a). Moreover, 25A mutants dramatically reduced or abrogated the binding with 241_2F04, 346-54, SFV009_3G01, and 222-1C06 since W14, H25, and Y34 form major hydrophobic contacts with HCDR3 in the upper and middle pockets. 25A was not as critical for interaction with S100a and S100b in 047-09_4F04 (Fig. 7a). The binding was also affected for all antibodies when I133 was substituted with A133, which is involved in the hydrophobic interaction between HA and antibodies in the middle pocket. These substitutions appear to disrupt the hydrophobic interaction in the upper and middle pockets with HCDR3. The A32 mutant, a major

https://doi.org/10.1038/s41467-025-56496-4

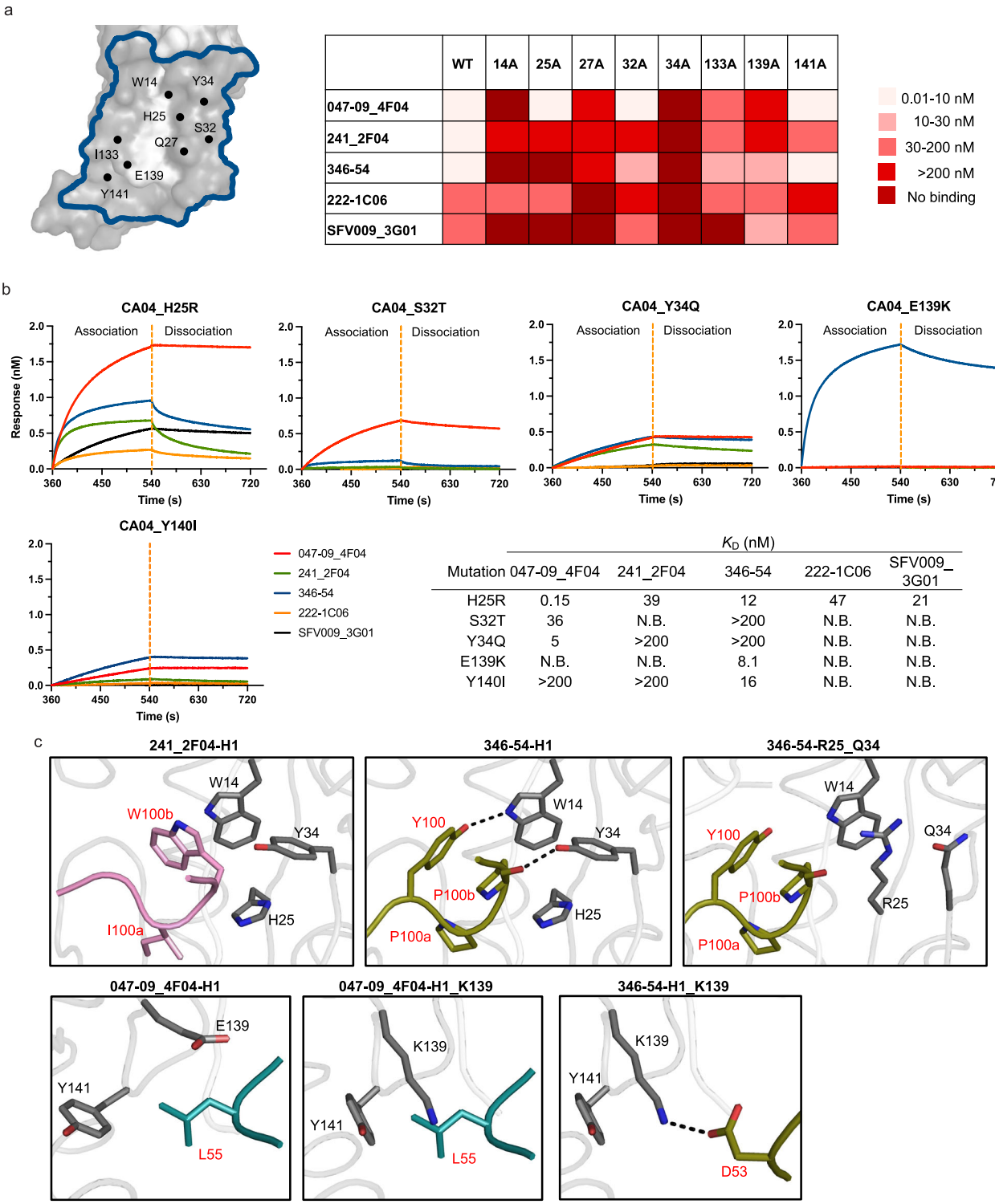


| Mutation | $K_D$ (nM) 047-09_4F04 | 241_2F04 | 346-54 | 222-1C06 | SFV009_3G01 |
|---|---|---|---|---|---|
| H25R | 0.15 | 39 | 12 | 47 | 21 |
| S32T | 36 | N.B. | >200 | N.B. | N.B. |
| Y34Q | 5 | >200 | >200 | N.B. | N.B. |
| E139K | N.B. | N.B. | 8.1 | N.B. | N.B. |
| Y140I | >200 | >200 | 16 | N.B. | N.B. |

**Fig. 7 | Differences in anchor epitope residues and genetic barrier between H1 and H3. a** The anchor epitope on CA04 H1N1 HA is shown as a blue outline on the HA molecular surface. HA residues for mutational substitution are labeled. Binding affinity of 047-09_4F04, 241_2F04, and 346-54 to each mutant was measured using biolayer interferometry (BLI) and depicted in different colors. In the binding assay, a Kd value > 200 nM indicates that only a very weak signal was detected at 250 nM concentration. **b** Binding Kd of each anchor antibody to HA mutants using BLI. Binding was measured for Fabs to each mutant at 250 nM. Residues that differ between A/California/04/2009 H1N1 (PDB: 4M4Y) and A/Hong Kong/1/1968 H3N2 (PDB: 4FNK) HA on the epitope of anchor antibodies were analyzed. N.B. represent no binding. Sensorgrams for binding are shown in Supplementary Fig. 15, 16. **c** Structural analysis of genetic differences in the middle and lower hydrophobic pockets between H1 and H3 HA. H25, Y34, and K139 were introduced into Apo-CA04 H1N1 HA (PDB: 4M4Y) using foldX, and the 047-09_4F04-H1 and 346-54-H1 complex was superimposed with Apo-CA04 H1_R25_Q34 and Apo-CA04_H1_K139. A possible salt bridge between K139 and D53 in 346-54 is indicated by black dashes.

residue making several hydrogen bonds with LCDR3, had a moderate effect on 047-09_4F04, 346-54, and SFV009_3G01, whereas the mutation substantially affects binding with 241_2F04 and 222-1C06. Residue Q27 also forms hydrogen bonds with Y58 from HCDR2 and W94 from LCDR3. When substituted with alanine, 27A severely affected the binding of all antibodies (Fig. 7a). These findings suggest that the main- and side-chain hydrogen bonds formed between Q27 and S32 and LCDR3 are critical. Alanine scanning of H1 HA at these contact residues revealed the possibility of escape mutations, although these residues are highly conserved in H1N1 HAs isolated from humans between 1918-2023 (Supplementary Fig. 9a).

Despite similarity (~50% overall identity) in the anchor epitope residues between H1N1 and H3N2 HA (Supplementary Fig. 9), none of the anchor antibodies were able to acquire cross-reactivity to group 2 HA. We further analyzed the genetic barriers for recognition of the anchor epitope between H1N1 and H3N2 HA via measuring binding after substitution of different residues from A/Hong Kong/1/1968 H3N2 (HK68) HA into CA04 H1N1 HA. We chose five residues involved in most interactions between the anchor antibodies and HA. The introduction of H25R into H1 HA reduced binding in all antibodies except 047-09_4F04. Mutations, Y34Q and Y140I, also decreased binding in all antibodies, generally to a greater extent (Fig. 7b). Since the H25R and Y34Q mutations are in the upper and middle hydrophobic pockets, the hydrophobic interactions between HA and HCDR3 are compromised (Fig. 7b). This result is also consistent with alanine scanning, suggesting that residues 25 and 34 are crucial residues for interaction between anchor antibodies and HA. When introducing S32T to H1 HA, threonine substantially affects the binding of 241_2F04, 346-54, SFV009_3G01, and 222-1C06 compared to 047-09_4F04 (Fig. 7b). E139 is a critical epitope residue for anchor antibodies binding with H1 HA and makes hydrogen bonds with serine residues in HCDR2, especially in 047-09_4F04 and 241_2F04 (Fig. 3a and b). E139K reverses the charge at this position and would abolish the interaction and, therefore, affect binding in 047-09_4F04 and 241_2F04 (Fig. 7c). In particular, hydrophobic interactions of SHM L/I55 in HCDR2 in 047-09_4F04 and 241_2F04 with the lower pocket would be diminished by the longer E193K extending into the hydrophobic pocket (Fig. 7c). Notably, in 346-54, K193 can be accommodated since there is no hydrophobic interaction between G55 and the lower pocket (Fig. 3c). D53 could then potentially form a salt bridge with K193 in 346-54 as visualized by modeling with FoldX[41] (Fig. 7c). Thus, there are genetic barriers for the anchor antibodies isolated to date to cross-react between H1 and H3 subtypes.

## Discussion

In the past decade, the concept of influenza vaccine development has changed from creating vaccines as quickly as possible, including mRNA delivery, to reproducible bnAb elicitation[16,42,43]. The bnAbs induced and observed in multiple individuals after vaccination are represented in multidonor antibody classes and are considered immunological solutions to more universal vaccine development against influenza viruses[44,45]. Multidonor class antibodies recognize a similar epitope region on HA using similar binding modes and similar genetic recombination and maturation pathways[28,44]. Over the last decade, several HA stem-binding bnAbs have been found that share similar genetic elements and have been identified in multiple donors, such as $V_H$1-69, $V_H$1-18, $V_H$6-1, and $V_H$3-30, as well as $D_H$3-9[24,33,46–50]. These stem-specific bnAbs are also protective against zoonotic H5N1 and H7N9 in animal studies[33,51]. In this study, our analysis provides further insight into the structural basis for antibodies recognizing the HA membrane-proximal anchor region through similar binding modes, although from different VDJ gene recombinations. In contrast to multidonor stem-binding bnAbs, which mostly share a comparable binding mode for HCDR3, these anchor antibodies target the anchor epitope primarily through several other features: a germline-encoded Y98 from HCDR2, a conserved NWPP motif from LCDR3, intra-aromatic interaction between HCDR2, HCDR3, and LCDR3, and targeting upper and middle pockets of the anchor epitope via hydrophobic residues at the tip of HCDR3[36,39,40]. Thus, the structurally convergent features derived from different $V_H$ ($V_H$3-23, $V_H$3-30, $V_H$3-30-3, and $V_H$3-48) and $V_K$ ($V_K$3-11 and $V_K$3-15) germlines appear to be a critical factor in antibody targeting of this conserved epitope, as demonstrated also by antibodies to SARS-CoV-2 (YYDRxG in HCDR3)[52] and HIV (antibodies targeting CD4 binding site)[53]. Notably, 346-54, isolated from a chimeric HA vaccine trial[16], has more variation in HCDR2 but still retains a similar binding mode, and displays neutralizing breadth and potency that rivals FI6v3 in H1N1 viruses[25], suggesting some amino acid tolerance in this convergent antibody structure. In light of the flexible angle that HA can adopt relative to the viral surface, the approach of anchor antibodies to the HA anchor epitope might then be more accessible when the HA is tilted relative to the membrane[40,54].

Given the central stem region is a subdominant target for broadly neutralizing antibodies, several mutations have arisen from selective pressure by antibodies against this epitope, resulting in the stem region being capable of escaping bnAbs[55–58]. Recently, a vaccine strategy that uses H2 and H5 as immunogens to induce anchor-specific memory B cells capable of neutralizing group 1 H1, H2, and H5 has been demonstrated[39]. Furthermore, the neutralization ability of anchor antibodies against a wide variety of H1N1 strains might provide a solution for seasonal and future H1N1 pandemics. Sequence analysis of anchor epitope residues in H1N1 and H3N2 revealed that these regions are highly conserved in each subtype. In addition, alanine scanning also indicated several residues were critical in the anchor epitope; the frequency of mutations in these residues was very low from 1918 to 2023 (Supplementary Fig. 9). Despite this relative conservation, residue substitutions from H3 into H1 HA abrogated binding among four anchor antibodies. Whether cross-reactive anchor bnAbs against group 2 viruses can be identified remains an open question, particularly whether they will also exhibit the same immunoglobulin gene use bias. Notwithstanding, convergent solutions to anchor antibodies with low levels of SHM have the potential to be robustly elicited through next-generation vaccine strategies in different individuals.

## Methods

### HA expression and purification

HAs for biolayer interferometry (BLI) analysis and structure determination were produced in insect cell expression systems following a previous protocol[59]. Each HA gene was incorporated into expression vector pFastbac-1 with an N-terminal gp67 signal peptide and a C-terminal trimerization followed by a thrombin cleavage and 6X his-tag. After the sequence was confirmed, the recombinant baculoviruses were generated using a bac-to-bac baculovirus system in Sf9 cells (Thermo Fisher Scientific). HA proteins were expressed in High Five cells with a multiplicity of infection (MOI) of 5-10 for each recombinant virus and harvested from supernatant after 72 hours. The harvested supernatant was further clarified by centrifugation. Soluble HA proteins were purified by metal-affinity chromatography using $Ni^{2+}$ resin and buffer-exchanged into 1X Tris-buffered saline (TBS, pH 8). The HA was treated with trypsin in a final ratio of 1:1000 (wt/wt) to produce uniformly cleaved HA1/HA2. The cleaved HA was further purified by size exclusion chromatography (SEC) using a Hiload 16/90 Superdex 200 column (GE Healthcare) for crystallization trials. The HA used for cryoEM was expressed using the expi293F expression system. Briefly, The HA (A/California/04/2009 with E47K stabilizing mutation in HA2) gene in pcDNA3.4 with C-terminal foldon trimerization domain and 6xHis tag was transfected in 300 mL expi293F culture. After 5 days, the supernatant was harvested, clarified, and run over the HisTrap column. The HA was trypsinized to cleave HA0 into HA1/HA2 and purified by SEC as described above.

### Antibody Fab expression and purification

The sequences of anchor antibodies that are listed in Supplementary Fig. 1 and selected in this study were isolated from prior studies of participants immunized with 2009 monovalent inactivated pandemic influenza vaccine (MIV), 2004-2015 quadrivalent inactivated influenza vaccine (QIV) or chimeric cH8/1 and cH5/1 influenza A group 1 cHA vaccine[16,17,36]. The sequences were used to express and purify recombinant antibody Fabs. The light and heavy chain variable domains of each Fab were synthesized and incorporated into a phCMV vector with human kappa $C_L$ and $C_H$ 1 regions, respectively. Fabs were expressed by transient co-transfection with heavy and light chain expression vectors into ExpoCHO cells (Thermo Fisher Scientific) at 37 °C with 8% $CO_2$ for one week. Recombinant Fabs were harvested from culture supernatant by affinity chromatography using CH1-XL beads followed by SEC using a Hiload 16/90 Superdex 200 column. Fractions containing purified Fab were concentrated and exchanged into pH 8.0 TBS buffer.

### Crystallization, data collection, and structure determination

To obtain HA-Fab structures, complexes were generated by mixing Fab in a 3-fold molar ratio with HA protomer (i.e. 3 Fabs per HA trimer) and incubated overnight at 4 °C. The HA-Fab complex was further purified by SEC using Superdex 200 10/300 column. The purified complex was subsequently diluted to ~8 mg/ml in pH 8.0 TBS buffer. The initial crystallization conditions for each Fab-HA complex were obtained from screening on our robotic high-throughput CrystalMation system (Rigaku) at The Scripps Research Institute using the JCSG Core Suite (QIAGEN) as precipitant. Crystallization screening was set up by sitting drop vapor diffusion method containing 0.1 µl of protein and 0.1 µl of reservoir solution. The optimized crystallization conditions were: 0.2 M sodium citrate pH 5.4, 18% PEG3350 for the 047-09-4F04-HA complex; 0.2 M sodium acetate pH 6.2, 20% PEG3350 for the 241-2F04-HA complex; and 0.2 M lithium sulfate pH 6.2, 16% PEG3350 for the 346-54-HA complex. Crystals were harvested after two weeks and then soaked in a reservoir solution with 12-18% (v/v) ethylene glycol as cryoprotectant. The harvested crystals were flash-cooled and stored in liquid nitrogen until data collection. Diffraction data for each HA-Fab complex were collected at synchrotron radiation beamlines specified on the crystal data statistics table (Supplementary Table 1). The diffraction data were processed with HKL2000[60]. The initial phases for the HA-Fab complex were solved by molecular replacement using Phaser with the models generated by Repertoire Builder (https://sysimm.org/rep_builder/) for each Fab and CA04 HA (4M4Y) as HA model[61]. Model building and refinement were completed in Coot and PHENIX[62,63], respectively. Buried and accessible surface areas were calculated with PISA[64]. Molecular surface contact areas were computed using the Molecular Surface package[65]. X-ray and cryo-EM data processing and refinement statistics are in Supplementary Tables 1 and 2.

### Cryo-EM sample preparation

HA-Fab complexes were prepared by mixing Fab in a 3:1 molar ratio with HA (i.e. 3 Fabs per HA trimer) and incubated overnight at 4 °C. 0.1% w/v octyl-beta-glucoside detergent was added to the complex to aid in particle tumbling. The final concentration of the sample was 0.7 mg/mL on the grid. A Vitrobot Mark IV system was used to prepare cryoEM grids. The settings were as follows: temperature inside the chamber was 25 °C, the humidity was 100%, blotting force was 1, wait time was 5 s, and blotting time was varied within a 3.5 to 5.5 s range. 3 µL of the sample was added to plasma cleaned 1.2/1.3 copper Quantifoil 300 mesh grid. The plasma cleaning step was performed in the Solarus 950 plasma system (Gatan) with $Ar/O_2$ gas mix for 25 s. The sample was blotted off for 4 s and the grids were plunge-frozen into liquid-nitrogen-cooled liquid ethane.

### Cryo-EM data collection, processing, and model building

Cryo grids of A/California/04/2009 (CA04)- SFV009_3G01 complexes were imaged at 190,000× nominal magnification using a Falcon 4i camera on a Glacios microscope at 200 kV. Automated image collection was performed using EPU from ThermoFisher. Images were aligned, dose-weighted, and Contrast Transfer Function (CTF)-corrected in the CryoSPARC Live™ software platform, with automated image collection also performed using Smart EPU software (ThermoFisher). Data processing for all three datasets was carried out in CryoSPARC v4.1.2[66]. Blob particle picking was performed on all micrographs with a minimum particle diameter of 100 Å and a maximum of 200 Å. Particles extracted at 512 pixels box size were used to perform 2D classification, which were then used to generate a 3D reference model from ab initio refinement, followed by heterogeneous refinement to obtain one good class that was further non-uniform (NU) heterogeneous refined. Gold-Standard Fourier Shell Correlation (GSFSC) resolution was calculated to be 2.9 Å. The resolution values are possibly overestimated due to some orientation bias and particle heterogeneity (Supplementary Fig. 10). Initial coordinates of SFV009_3G01 were generated using ABodyBuilder2[67] and for the HA model we used the PDB 7T3D as initial template[36]. We docked the models into the cryoEM density map in UCSF ChimeraX[68]. The structure model was built iteratively with COOT followed by real-space refinement in PHENIX package[69]. The Kabat numbering system[70] was used for mAb and the H3 numbering scheme for HA.

### Binding ability and affinity measurement

The binding of each Fab to HA was evaluated with BLI using an Octet Red instrument. For binding assays, Fabs were used at 20 µg/ml in 1× kinetics buffer (1× PBS, pH 7.4, 0.01% BSA, and 0.002% Tween 20) and loaded onto F2G biosensors and incubated with HA in 1× kinetics buffer. For the binding affinity assay, HA at 20 µg/ml in 1× kinetics buffer was loaded onto nickel-nitrilotriacetic acid (Ni-NTA) biosensors and measured with Fabs at 2-fold serial dilution starting from 250 nM. Experiments were performed at 22 °C and data were fit with a 1:1 binding model.

### Micro-neutralization assay

Madin-Darby canine kidney cells with the cDNA of human 2,6-sialtransferase (SIAT1-MDCK) were seeded onto 96-well plates with $1\times10^5$ cells/ml in each well. After cell seeding, plates were incubated overnight at 37°C in 5% $CO_2$. Cells were washed with Phosphate-buffered saline (PBS) twice, and the medium was replaced with 100 µL an improved reduced-serum minimal essential medium (OptiMEM) containing 1 µg/ml tosylamido-2-phenylethyl chloromethyl ketone (TPCK-treated) trypsin. 50 µg of each antibody was serially diluted threefold in 50 Tissue Culture Infectious Dose ($TCID_{50}$) virus diluent. The mixtures were then transferred to 96-well plates. The assay for each antibody was performed in triplicate and incubated with cells at 37°C for 72 hours in a 5% $CO_2$ incubator. CellTiter-Glo 2.0 luminescent cell viability reagent (Promega) was then added to each well based on the manufacturer's instructions. Luminescence was measured on a TECAN plate reader, and half maximal effective concentration ($EC_{50}$) values were calculated with GraphPad Prism 10 (n = 3 for each condition). H1N1 viruses used in this assay were: A/Puerto Rico/8/1934 (PR8), A/Marton/1943, A/Beijing/262/1995, A/USSR/90/1977, A/Solomon Islands/3/2006, A/California/04/2009 (CA04), A/Michigan/45/2015, and A/Hawaii/70/2019.

### Thermal stability assay

The wild type and mutant Fabs for this assay were expressed in Expi-CHO cells (Thermo Fisher Scientific). Samples were diluted into TBS with the final concentration at 300ug in the reaction. TBS without protein was used as a control. The sensor was washed twice with buffer before proceeding to the next sample. The reaction was set up from

20°C and heated up to 100 °C in a scan rate of 90 °C/hr. The data were analyzed with buffer correction, normalization, and baseline subtraction by Origin 7.0 software.

### Immunoglobulin heavy and light chain sequences analysis

Germline gene usage, complementarity-determining regions (CDRs) analysis, VDJ gene rearrangement, and sequence identity to its germline for each anchor antibody were analyzed in IgBLAST[71] and international ImMunoGeneTics information system (IMGT)[72]. Kabat numbering of each Fab was carried out using abYsis[73].

### Reporting summary

Further information on research design is available in the Nature Portfolio Reporting Summary linked to this article.

## Data availability

All data are presented in the paper. The X-ray coordinates, structure statistics, and cryoEM model have been deposited in the Research Collaboratory for Structural Bioinformatics (RCSB) Protein Data Bank under accession codes 9DRU for CA04 H1 HA in complex with 047-09_4F04, 9DS1 for CA04 H1 HA in complex with 241_2F04, 9DS2 for CA04 H1 HA in complex with 346-54, 9DS3 for Apo-241_2F04, 9DSC for Apo-241_2F04-A95a, and 9DM0 for CA09 H1 HA in complex with SFV009_3G01. The cryoEM structure and corresponding data have been deposited to the Electron Microscopy DataBank under accession EMD-46994. All other studies are included in the main text and/or *SI Appendix*. Source data are provided with this paper.

## References


1. World Health Organization. Influenza (Seasonal). https://www.who.int/news-room/fact-sheets/detail/influenza-(seasonal) (3 October 2023).
2. Wu, N. C. & Wilson, I. A. A perspective on the structural and functional constraints for immune evasion: insights from influenza virus. *J. Mol. Biol.* **429**, 2694–2709 (2017).
3. Claas, E. C. et al. Human influenza A H5N1 virus related to a highly pathogenic avian influenza virus. *Lancet* **351**, 472–477 (1998).
4. Gao, R. et al. Human infection with a novel avian-origin influenza A (H7N9) virus. *N. Engl. J. Med* **368**, 1888–1897 (2013).
5. Chen, H. et al. Clinical and epidemiological characteristics of a fatal case of avian influenza A H10N8 virus infection: a descriptive study. *Lancet* **383**, 714–721 (2014).
6. Uyeki, T. M. et al. Highly pathogenic avian influenza A(H5N1) virus infection in a dairy farm worker. *N. Engl. J. Med* **390**, 2028–2029 (2024).
7. Lin, T. H. et al. A single mutation in bovine influenza H5N1 hemagglutinin switches specificity to human receptors. *Science* **386**, 1128–1134 (2024).
8. Garten, R. J. et al. Antigenic and genetic characteristics of swine-origin 2009 A(H1N1) influenza viruses circulating in humans. *Science* **325**, 197–201 (2009).
9. Wu, Y., Wu, Y., Tefsen, B., Shi, Y. & Gao, G. F. Bat-derived influenza-like viruses H17N10 and H18N11. *Trends Microbiol* **22**, 183–191 (2014).
10. Tong, S. et al. A distinct lineage of influenza A virus from bats. *Proc. Natl Acad. Sci. USA* **109**, 4269–4274 (2012).
11. Fereidouni, S. et al. Genetic characterization of a new candidate hemagglutinin subtype of influenza A viruses. *Emerg. Microbes Infect.* **12**, 2225645 (2023).
12. Karakus, U. et al. H19 influenza A virus exhibits species-specific MHC class II receptor usage. *Cell Host Microbe* **32**, 1089–1102.e10 (2024).
13. Tong, S. et al. New world bats harbor diverse influenza A viruses. *PLoS Pathog.* **9**, e1003657 (2013).
14. Wu, N. C. & Wilson, I. A. Structural insights into the design of novel anti-influenza therapies. *Nat. Struct. Mol. Biol.* **25**, 115–121 (2018).
15. Wu, N. C. & Wilson, I. A. Influenza hemagglutinin structures and antibody recognition. *Cold Spring Harb. Perspect. Med* **10**, a038778 (2020).
16. Nachbagauer, R. et al. A chimeric hemagglutinin-based universal influenza virus vaccine approach induces broad and long-lasting immunity in a randomized, placebo-controlled phase I trial. *Nat. Med* **27**, 106–114 (2021).
17. Bernstein, D. I. et al. Immunogenicity of chimeric haemagglutinin-based, universal influenza virus vaccine candidates: interim results of a randomised, placebo-controlled, phase 1 clinical trial. *Lancet Infect. Dis.* **20**, 80–91 (2020).
18. Andrews, S. F. et al. A single residue in influenza virus H2 hemagglutinin enhances the breadth of the B cell response elicited by H2 vaccination. *Nat. Med* **28**, 373–382 (2022).
19. Impagliazzo, A. et al. A stable trimeric influenza hemagglutinin stem as a broadly protective immunogen. *Science* **349**, 1301–1306 (2015).
20. Krammer, F. & Palese, P. Advances in the development of influenza virus vaccines. *Nat. Rev. Drug Discov.* **14**, 167–182 (2015).
21. Ekiert, D. C. et al. Antibody recognition of a highly conserved influenza virus epitope. *Science* **324**, 246–251 (2009).
22. Kashyap, A. K. et al. Combinatorial antibody libraries from survivors of the Turkish H5N1 avian influenza outbreak reveal virus neutralization strategies. *Proc. Natl Acad. Sci. USA* **105**, 5986–5991 (2008).
23. Ekiert, D. C. et al. A highly conserved neutralizing epitope on group 2 influenza A viruses. *Science* **333**, 843–850 (2011).
24. Dreyfus, C. et al. Highly conserved protective epitopes on influenza B viruses. *Science* **337**, 1343–1348 (2012).
25. Corti, D. et al. A neutralizing antibody selected from plasma cells that binds to group 1 and group 2 influenza A hemagglutinins. *Science* **333**, 850–856 (2011).
26. Pappas, L. et al. Rapid development of broadly influenza neutralizing antibodies through redundant mutations. *Nature* **516**, 418–422 (2014).
27. Wheatley, A. K. et al. H5N1 vaccine-elicited memory B cells are genetically constrained by the IGHV locus in the recognition of a neutralizing epitope in the hemagglutinin stem. *J. Immunol.* **195**, 602–610 (2015).
28. Joyce, M. G. et al. Vaccine-induced antibodies that neutralize group 1 and group 2 influenza A viruses. *Cell* **166**, 609–623 (2016).
29. Wu, N. C. et al. Convergent evolution in breadth of two $V_H$6-1-encoded influenza antibody clonotypes from a single donor. *Cell Host Microbe* **28**, 434–444.e4 (2020).
30. Wu, N. C. et al. Recurring and adaptable binding motifs in broadly neutralizing antibodies to influenza virus are encoded on the D3-9 segment of the Ig gene. *Cell Host Microbe* **24**, 569–578.e4 (2018).
31. Ellebedy, A. H. et al. Induction of broadly cross-reactive antibody responses to the influenza HA stem region following H5N1 vaccination in humans. *Proc. Natl Acad. Sci. USA* **111**, 13133–13138 (2014).
32. Wang, T. T. et al. Broadly protective monoclonal antibodies against H3 influenza viruses following sequential immunization with different hemagglutinins. *PLoS Pathog.* **6**, e1000796 (2010).
33. Andrews, S. F. et al. Preferential induction of cross-group influenza A hemagglutinin stem-specific memory B cells after H7N9 immunization in humans. *Sci. Immunol.* **2**, eaan2676 (2017).
34. Guthmiller, J. J. et al. First exposure to the pandemic H1N1 virus induced broadly neutralizing antibodies targeting hemagglutinin head epitopes. *Sci. Transl. Med* **13**, eabg4535 (2021).
35. Yassine, H. M. et al. Hemagglutinin-stem nanoparticles generate heterosubtypic influenza protection. *Nat. Med* **21**, 1065–1070 (2015).
36. Guthmiller, J. J. et al. Broadly neutralizing antibodies target a haemagglutinin anchor epitope. *Nature* **602**, 314–320 (2022).
37. Andrews, S. F. et al. Immune history profoundly affects broadly protective B cell responses to influenza. *Sci. Transl. Med* **7**, 316ra192 (2015).

38. Li, G. M. et al. Pandemic H1N1 influenza vaccine induces a recall response in humans that favors broadly cross-reactive memory B cells. *Proc. Natl Acad. Sci. USA* **109**, 9047–9052 (2012).
39. Andrews, S. F. et al. An influenza H1 hemagglutinin stem-only immunogen elicits a broadly cross-reactive B cell response in humans. *Sci. Transl. Med* **15**, eade4976 (2023).
40. Benton, D. J. et al. Influenza hemagglutinin membrane anchor. *Proc. Natl Acad. Sci. USA* **115**, 10112–10117 (2018).
41. Schymkowitz, J. et al. The FoldX web server: an online force field. *Nucleic Acids Res* **33**, W382–W388 (2005).
42. Dunkle, L. M. & Izikson, R. Recombinant hemagglutinin influenza vaccine provides broader spectrum protection. *Expert Rev. Vaccines* **15**, 957–966 (2016).
43. Cox, M. M. & Hollister, J. R. FluBlok, a next generation influenza vaccine manufactured in insect cells. *Biologicals* **37**, 182–189 (2009).
44. Andrews, S. F. & McDermott, A. B. Shaping a universally broad antibody response to influenza amidst a variable immunoglobulin landscape. *Curr. Opin. Immunol.* **53**, 96–101 (2018).
45. Sangesland, M. et al. Germline-encoded affinity for cognate antigen enables vaccine amplification of a human broadly neutralizing response against influenza virus. *Immunity* **51**, 735–749.e8 (2019).
46. Sui, J. et al. Structural and functional bases for broad-spectrum neutralization of avian and human influenza A viruses. *Nat. Struct. Mol. Biol.* **16**, 265–273 (2009).
47. Lang, S. et al. Antibody 27F3 broadly targets influenza A group 1 and 2 hemagglutinins through a further variation in $V_H$1-69 antibody orientation on the HA stem. *Cell Rep.* **20**, 2935–2943 (2017).
48. Wu, Y. et al. A potent broad-spectrum protective human monoclonal antibody crosslinking two haemagglutinin monomers of influenza A virus. *Nat. Commun.* **6**, 7708 (2015).
49. Fu, Y. et al. A broadly neutralizing anti-influenza antibody reveals ongoing capacity of haemagglutinin-specific memory B cells to evolve. *Nat. Commun.* **7**, 12780 (2016).
50. Kallewaard, N. L. et al. Structure and function analysis of an antibody recognizing all influenza A subtypes. *Cell* **166**, 596–608 (2016).
51. Throsby, M. et al. Heterosubtypic neutralizing monoclonal antibodies cross-protective against H5N1 and H1N1 recovered from human $IgM^+$ memory B cells. *PLoS One* **3**, e3942 (2008).
52. Liu, H. et al. Human antibodies to SARS-CoV-2 with a recurring YYDRxG motif retain binding and neutralization to variants of concern including Omicron. *Commun. Biol.* **5**, 766 (2022).
53. Zhou, T. et al. Structural repertoire of HIV-1-neutralizing antibodies targeting the CD4 supersite in 14 donors. *Cell* **161**, 1280–1292 (2015).
54. Amaro, R. E. et al. A computational assay that explores the hemagglutinin/neuraminidase functional balance reveals the neuraminidase secondary site as a novel anti-influenza target. *ACS Cent. Sci.* **4**, 1570–1577 (2018).
55. Wu, N. C. et al. Different genetic barriers for resistance to HA stem antibodies in influenza H3 and H1 viruses. *Science* **368**, 1335–1340 (2020).
56. Chai, N. et al. Two escape mechanisms of influenza A virus to a broadly neutralizing stalk-binding antibody. *PLoS Pathog.* **12**, e1005702 (2016).
57. Roubidoux, E. K. et al. Mutations in the hemagglutinin stalk domain do not permit escape from a protective, stalk-based vaccine-induced immune response in the mouse model. *mBio* **12**, e03617–e03620 (2021).
58. Prachanronarong, K. L. et al. Mutations in influenza A virus neuraminidase and hemagglutinin confer resistance against a broadly neutralizing hemagglutinin stem antibody. *J. Virol.* **93**, e01639–18 (2019).
59. Stevens, J. et al. Structure and receptor specificity of the hemagglutinin from an H5N1 influenza virus. *Science* **312**, 404–410 (2006).
60. Otwinowski, Z. & Minor, W. Processing of X-ray diffraction data collected in oscillation mode. *Methods Enzymol.* **276**, 307–326 (1997).
61. McCoy, A. J. et al. Phaser crystallographic software. *J. Appl Crystallogr* **40**, 658–674 (2007).
62. Emsley, P., Lohkamp, B., Scott, W. G. & Cowtan, K. Features and development of Coot. *Acta Crystallogr D. Biol. Crystallogr* **66**, 486–501 (2010).
63. Adams, P. D. et al. PHENIX: a comprehensive python-based system for macromolecular structure solution. *Acta Crystallogr D. Biol. Crystallogr* **66**, 213–221 (2010).
64. Krissinel, E. & Henrick, K. Inference of macromolecular assemblies from crystalline state. *J. Mol. Biol.* **372**, 774–797 (2007).
65. Connolly, M. L. Analytical molecular surface calculation. *J. Appl Crystallogr* **16**, 548–558 (1983).
66. Punjani, A., Rubinstein, J. L., Fleet, D. J. & Brubaker, M. A. cryoSPARC: algorithms for rapid unsupervised cryo-EM structure determination. *Nat. Methods* **14**, 290–296 (2017).
67. Abanades, B. et al. ImmuneBuilder: Deep-Learning models for predicting the structures of immune proteins. *Commun. Biol.* **6**, 575 (2023).
68. Pettersen, E. F. et al. UCSF ChimeraX: Structure visualization for researchers, educators, and developers. *Protein Sci.* **30**, 70–82 (2021).
69. Afonine, P. V. et al. Real-space refinement in PHENIX for cryo-EM and crystallography. *Acta Crystallogr D. Struct. Biol.* **74**, 531–544 (2018).
70. Kabat, E. A., Wu, T. T., Bilofsky, H. & National Institutes of, H. *Sequences of immunoglobulin chains: tabulation and analysis of amino acid sequences of precursors, V-regions, C-regions, J-chain and $\beta_2$-microglobulins, 1979*, xv, 185 p. (U. S. Dept. of Health, Education, and Welfare, Public Health Service, National Institutes of Health, Bethesda, Md., 1979).
71. Ye, J., Ma, N., Madden, T. L. & Ostell, J. M. IgBLAST: an immunoglobulin variable domain sequence analysis tool. *Nucleic Acids Res* **41**, W34–W40 (2013).
72. Lefranc, M. P. et al. IMGT, the international ImMunoGeneTics information system. *Nucleic Acids Res* **37**, D1006–D1012 (2009).
73. Swindells, M. B. et al. abYsis: integrated antibody sequence and structure-management, analysis, and prediction. *J. Mol. Biol.* **429**, 356–364 (2017).


## Acknowledgements

We thank Henry Tien for helping with the automated robotic crystal screening at The Scripps Research Institute. The research here was supported by the NIH National Institute of Allergy and Infectious Diseases (NIAID) Collaborative Influenza Vaccine Innovation Centers (CIVICs) contract grant 75N93109C00051 (to I.A.W., A.B.W., F.K. and P.C.W.). We are grateful to the staff at the Advanced Photon Source (APS) beamline 23ID-D and 23ID-B (GM/CA CAT), Stanford Synchrotron Radiation Lightsource (SSRL) beamline 12-1, and National Synchrotron Light Source II (NSLS-II) beamlines 17-ID-1, where X-ray diffraction datasets were collected. GM/CA CAT is funded in whole or in part with federal funds from the National Cancer Institute (Y1-CO-1020) and the National Institute of General Medical Sciences (NIGMS) (Y1-GM-1104). Use of the APS was supported by the US Department of Energy (DOE), Basic Energy Sciences, Office of Science, under Contract DE-AC02-06CH11357. The SSRL is a Directorate of SLAC National Accelerator Laboratory, and an Office of Science User Facility operated for the US DOE of Science by Stanford University. The SSRL Structural Molecular Biology Program is supported by the DOE Office of Biological and Environmental Research, and by the NIH, NIGMS (including P41GM103393), and the National Center for Research Resources (NCRR) (P41RR001209). This research used resources of the National Synchrotron Light Source II, a U.S. Department of Energy (DOE) Office of Science

User Facility operated for the DOE Office of Science by Brookhaven National Laboratory under Contract No. DE-SC0012704. The contents of this publication are solely the responsibility of the authors and do not necessarily represent the official views of NIAID, NIGMS, NCRR, or NIH.

## Author contributions

T.H.L., X.Z., A.B.W., and I.A.W. conceived experiments. Antibody sequences were provided by J.J.G., F.K., and P.C.W. T.H.L., C.C.D.L., and W.Y. prepared recombinant proteins and Fabs. T.H.L. collected and analyzed X-ray data and measured the binding affinities. T.H.L. and C.C.D.L. performed neutralization assays. M.L.F-Q., J.A.F., and J.H. performed cryo-EM. T.H.L. and I.A.W. wrote the original manuscript. All authors reviewed and edited the manuscript.

## Competing interests

The authors declare the following competing interests. Florian Krammer is listed as a co-inventor on patent applications filed by The Icahn School of Medicine at Mount Sinai relating to SARS-CoV-2 serological assays, NDV-based SARS-CoV-2 vaccines, influenza virus vaccines, and influenza virus therapeutics. Mount Sinai has spun out a company, Kantaro, to market serological tests for SARS-CoV-2 and another company, Castlevax, to develop SARS-CoV-2 vaccines. Florian Krammer is a co-founder and scientific advisory board member of Castlevax. Florian Krammer has consulted for Merck, CureVac, Seqirus, GSK, and Pfizer and is currently consulting for 3rd Rock Ventures, Sanofi, Gritstone and Avimex. The Krammer laboratory is also collaborating with Dynavax on influenza vaccine development. Patrick Wilson and Jenna Guthmiller are listed as co-inventors on a patent application filed by the University of Chicago relating to anchor epitope targeting antibodies. The remaining Authors have no competing interests to declare.

## Additional information

**Supplementary information** The online version contains supplementary material available at https://doi.org/10.1038/s41467-025-56496-4.

**Correspondence** and requests for materials should be addressed to Andrew B. Ward or Ian A. Wilson.

**Peer review information** *Nature Communications* thanks Donald Benton, and the other, anonymous, reviewer(s) for their contribution to the peer review of this work. A peer review file is available.